Forcespun metal oxide ultrafine tubes for hazardous gas monitoring

Omar Bouaaliouat, Houda Lahlou, Es-Said Akhouayri, Ahmed Ihlal, Abdeljalil Benlhachemi, Daniel Prades, Vanessa Fierro, Alain Celzard, Franck Berger, Jean-Baptiste Sanchez

Forcespun metal oxide ultrafine tubes for hazardous gas monitoring

Omar Bouaaliouat[a], Houda Lahlou[a*], Es-Said Akhouayri[a], Ahmed Ihlal[b], Abdeljalil Benlhachemi[c], Daniel Prades[d], Vanessa Fierro[e], Alain Celzard[e], Franck Berger[f], Jean-Baptiste Sanchez[f]

[a]*LETSMP laboratory-Faculty of Science-UIZ, Agadir 80000, Morocco*
[b]*LMER laboratory-Faculty of Science-UIZ, Agadir 80000, Morocco*
[c]*LME laboratory-Faculty of Science-UIZ, Agadir 80000, Morocco*
[d]*Département of Electronic and Biomedical Engineering-UB, Barcelona, Spain*
[e] *N2EV Department-Institut Jean Lamour, UMR 7198 CNRS-UL, Epinal, France*
[f] *MINAMAS Team, MN2S Department, UFR-ST, UFC-Besançon, France*

Abstract

In this paper, a simple home-made Forcespinning system was designed and successfully applied for the production of different metal oxide ultrafine tubes such as SnOx and ZnO. The morphology, purity, crystallinity and porosity of the forcespun samples were investigated by SEM, XRD, and EDS, TGA, and BET analysis. The samples were deposited unto a microsensing platform and their gas-sensing properties against different hazardous vapors such as ethanol, acetone and benzene were studied through preliminary tests at different detection temperatures. The results revealed different sensing behaviors of the prepared sensors towards the different vapors. Interestingly, the gas sensor based on SnO_x exhibited a higher and faster sensor response towards ethanol at 180°C as operating temperature. On the other hand, ZnO presented a higher response to acetone at 250°C. The ability of the prepared sensors to discriminate between the different vapors was explored.

Keywords: Forcespinning; metal oxide; ultrafine tubes; gas sensor; hazardous gas detection; Principal Component Analysis.

1. Introduction

Due to the fast growing of population and industrial facilities, gas detection systems can make a valuable contribution for precise monitoring and alerting of hazardous species related to human health, security or environmental issues [1].

Among the large inventory of hazardous substances, Acetone, Ethanol and Benzene are representative types of volatile organic compounds which can be found at high levels in indoor air [2-4]. Being widely used as laboratory reagents or as raw materials for the manufacture of different industrial products (such as adhesives, paints, cosmetics, detergents, etc.), these compounds may induce several short and long term exposure risks, especially for employers working in situ or people handling such products.

Following the National Institute for Occupational Safety and Health (NIOSH), exposure at low levels of Acetone can cause nose, eye and throat irritation, whereas at high level exposure, it can induce nervous system poisoning [2]. For Ethanol, short exposure can cause fatigue and nausea, whereas repeated exposure can affect the nervous system and the liver [3]. Also, Benzene can induce several respiratory problems and nervous damages at short term high level exposure, and may even lead to leukemia at longer exposure periods [4]. Moreover their health impacts, these compounds can induce safety risks due to their high flammability and explosive character when mixed with air.

In this sense, NIOSH has defined the maximum time weighted average (TWA) exposure limit for 10-hour workday as 250 ppm for Acetone and 1000 ppm for Ethanol, whereas for Benzene its TWA is estimated to 0.1 ppm [2-4]. However, a short term exposure limit of 250 ppm of benzene may induce cancer effects [4]. These levels are well under the threshold concentrations of flammability of such compounds in air. Hence, the detection at the ppm level is usually recommended.

* Corresponding author.
E-mail address: h.lahlou@uiz.ac.ma

Up to date, conductometric gas sensors based on metal oxide semiconductors (MOs) have been proved to be an excellent low cost and simple choice for the detection and monitoring of such gaseous species in various application fields such as food quality control, biomedical diagnosis (breath analysis), indoor and outdoor air quality monitoring and control of hazardous agents in industrial facilities, etc [5].
Recently, the controllable synthesis of one dimensional MOs nanomaterial's such as nanotubes, nanofibres, nanowires, has attracted much attention due to the fact that their physical and chemical properties are affected by their reduced dimensionality and size [6]. Moreover, they have been shown to be excellent materials for advanced applications including gas sensors for hazardous gas monitoring [7].
More particularly, 1D MOs nanotubes should provide large sensitivity because of their large length-to-diameter ratio and surface-to volume ratio. Up to now different metal oxide nanotubes, such as ZnO and SnO_2, have been synthesized through different methods such as reactive evaporation [8], atomic layer deposition method [9], Template assisted sol gel growth [10], Hydrothermal method [11-12], by electrodeposition [13] or by using the electrospinning technique [14-15], etc.

Of these, electrospinning provides a versatile route for the synthesis of functional nanotubes with a high porosity that includes both small and large pores being ideally suited for gas sensing [14-16]. However, this technique has some shortcomings such as slow production rate and high technical requirements, moreover the safety issues induced by the handling of high voltage supplies.

As alternative, Forcespinning, also known as "rotary jet spinning" is a recently developed fiber forming technique which has drawn an extensive attention, mainly due to its much higher production than electrospinning, its ease of use and safety, more especially because Forcespinning uses centrifugal force instead of electrical field for the production of ultrafine fibers [17]. All these features make it very promising for large industrial scale manufacturing of sensing devices.

Numerous works have proved that Forcespinning could be used to produce different polymer fibers ranging from the micro to nanoscale [18-19]. However the preparation of metal oxide fibers by Forcespinning is still rare. More particularly, to our best of knowledge, the synthesis of neither zinc oxide nor tin oxide nanotubes/nanofibers by this technique have been reported before.

In this work, SnO_x and ZnO are successfully produced by a home-made Forcespinning system. The different parameters of the Forcespinning process were adjusted so as to provide the appropriate conditions for fabricating ultrafine tubes. Then, the gas sensing properties of the forcespun SnO_x and ZnO samples towards different types of hazardous vapors at the ppm level, such as benzene, acetone and ethanol were investigated.

2. Experimental

2.1. Fiber formation procedure

SnO_x and ZnO were prepared by combining sol gel and forcespinning using tin chloride dihydrate ($SnCl_2$, 2 H_2O) and zinc acetate dihydrate (Zn $[COOCH_3]_2 \cdot 2H_2O$) as MOs precursors respectively and PolyviylPirrolidone (PVP MW 1300000) as fiber molding polymer.
Firstly, solution (S_1) was prepared by dissolving $SnCl_2$,$2H_2O$ or Zn $[COOCH_3]_2 \cdot 2H_2O$ in a mixture of ethanol /N,N-dimethylformamide (ratio 1:1) at 15 wt%. Meanwhile (S_2) was prepared by dissolving a certain amount of PVP in a mixture of ethanol/N, N-dimethylformamide (weight ratio 1:1) at 33 wt %, followed by magnetic stirring for 2 h at room temperature. Subsequently, (S_1) was added drop-wise to (S_2) and stirred for 2 h until the mixed solution (S_3) became clear.

A home-made Forcespinning system was designed for ultrafine MOs fiber preparation, as can be seen in figure 1. It relies on a stainless steel rotating reservoir with two symmetrical outlet nozzles with an internal diameter of 200 µm. The reservoir was surrounded with collecting metallic bars for allowing fiber collection during jet process.
In this sense, solution (S_3) was poured inside the forcespinning reservoir and ejected onto the collectors at room temperature under the effect of centrifugal force. In this process, the fibers were quickly transformed into fine fibers due to stretching induced by centrifugal force and evaporation of the solvent. In order to exhibit a stable jet initiation, the optimal nozzle-collector distance and the reservoir rotation speed were set to 10 cm and 10,000 rpm respectively. The As-spun PVP fibers were then annealed at 600 C ° with a heating rate of 5 °C/min for 5 h in order to completely remove polymer residues and allow metal precursors to oxidize and crystallize into MOs nanocrystals.

2.2. Material characterization

The morphology and composition of the prepared MOs samples were investigated by means of Field Emission Scanning Electron Microscopy combined with Energy dispersive X-ray Spectroscopy analysis (EDS) using a JEOL JSM-6700F FESEM microscope.
Nitrogen adsorption isotherms at -196°C were obtained using Micromeritics ASAP 2020 adsorption device. Before analysis, the samples were outgassed at 280°C. Then, the specific surface areas of both annealed SnO_x and ZnO samples were determined from N_2 adorption isotherms by applying the Brunauer-Emmett-Teller (BET) equation to obtain the specific surface area of each sample.
ThermoGravimetric Analysis and Differential Thermal Analysis (TGA-DTA; Netzsch STA44F3A9) were also used to investigate the thermal behavior of the as-deposited samples subjected to a thermal heating in air from room temperature to 1000 °C at a rate of 5°C/min.
Whereas X-Ray Diffraction (XRD) patterns were obtained using a Bruker D8 advanced X-ray diffractometer with Cu-Kα radiation (λ = 1.54060 Å). The average particle size of annealed MOs nanocrystals was calculated according to the Debye-Scherer formula.

2.3. Electrical characterization and data processing

The gas sensing properties of the prepared SnO_x and ZnO forcespun materials were studied using a conductometric characterization circuit (fig. 2a). For that, the MOs forcespun powders were deposited on a glass microsensing platform with interdigitated gold electrodes separated by a 10µm-gap (fig. 2b).

Afterwards, the prepared sensors were inserted inside a closed chamber equipped with gas inlet and outlet connectors and a rotating fun. Pure air was generated using dry air generator and served as carrier gas through the sensing chamber during the whole measurement cycle. The air flow across the chamber was maintained stable at 50 sccm using a Mass flow controller (MFC) system. The target vapor was injected into the test chamber with defined concentration using a micro-syringe.
Sensor response against gas was studied measuring the resistance of the devices using a voltage dividing circuit. Data acquisition was performed by a NI-DAQ acquisition card controlled through a Labview interface.
The sensor response was defined as the ratio $\left|\frac{R_g - R_a}{R_a}\right| * \mathbf{100}$, where Ra and Rg are the resistance of the sensor in reference pure air and after exposure to target vapor, respectively. Whereas the response time was defined as the time to reach 90% of the total resistance change in the gas adsorption stage.

The sensitivity of the sensor based on SnO_x and ZnO ultrafine fibers was investigated by measuring the sensor response against some typical toxic volatile organic vapors (VOCs), including Ethanol, Acetone, and Benzene at various sensor working temperatures at a fixed concentration for each vapor. From the calculated response magnitudes and response times, a data matrix was generated. A mathematical transformation method based on Principal Component Analysis (PCA) was then applied to evaluate the ability of combining a multisensing array based on ZnO and SnOx sensors operated at different temperatures to distinguish between the three target vapors according to their nature.
PCA was performed on the three vapor individuals with the aim to extract the interesting part of the information from the data matrix and represent it in a two-dimensional diagram whose coordinates were denoted as principal component 1 and principal component 2 [20].

3. Results and discussion

3.1. Morphological analysis

Fig.3 shows the FESEM images of the as-deposited $SnCl_2$/PVP and Zn $[COOCH_3]_2$ / PVP fibers and their thermally annealed SnO_x and ZnO counterparts respectively.
It can be clearly observed that the average diameter of the annealed samples dropped after annealing due to the removal of the PVP polymer and solvent residues. After annealing, the texture of the fibers was well maintained while showing a sub-micron and nano-tubular morphology averagely distributed around 6 µm for SnO_x and 700 nm

for ZnO respectively (fig 3e and f).

3.2. Thermal and compositional analysis

TGA-DTA analysis made on the as-deposited samples show that all volatiles such as H_2O, ethanol, DMF and organic components of PVP were completely removed below 580°C for $SnCl_2$/PVP composite (fig.4 a), and below 500 °C for Zn $[COOCH_3]2/$PVP composite (fig.4b), which confirmed the efficiency of the chosen post-thermal annealing process performed at 600 °C on the forcespun fibers.

Hence, the first minor weight loss before 180°C corresponds to the removal of free solvents in the precursors. While the significant weight loss of approximately 61%, between 180°C and 580°C (fig.4a), was attributed to the complete decomposition of $SnCl_2$ and degradation of PVP. Also, the significant weight loss observed in fig.4b of approximately 65% between 180°C and 500°C was attributed to the complete decomposition of Zn $[COOCH_3]_2$ and degradation of PVP.

This was further confirmed by elemental analysis performed on the annealed samples which demonstrated the presence of Sn and O elements for SnO_x, and Zn and O elements for ZnO after annealing, without any detected impurity or contamination (Fig. 5).

3.3. Structural and BET analysis

XRD measurements were carried out with the aim to investigate the crystal structure of the annealed samples at 600°C. On one hand, the analysis obtained show that the prepared SnO_x tubes are pure with an average grain size around 27.13 nm and crystallize into a unique phase corresponding to the tetragonal rutile SnO_x (fig.6 a), in accordance with the standard COD database values (code: 1521419). On the other hand, the analysis made on ZnO (fig.6 b) show that the prepared tubes are pure with an average grain size around 30.87 nm and crystallize into the hexagonal phase, in agreement with the standard COD database values (code: 9004181).

Furthermore, the results of BET analysis of N_2 adsorption isotherms depicted in figure 7 showed that the specific surface area of the MOs tubes was 38 m^2/g and 71 m^2/g for SnO_x and ZnO respectively, which supported the high porosity observed by FESEM analysis in case of ZnO tubes (fig. 3d).

3.4. Gas detection properties

It is well known that the operating temperature highly influences the response of semiconductor gas sensors. To determine the optimum operating temperature, the response of the fabricated gas sensors toward 18 ppm of ethanol, acetone and benzene in air was studied versus temperature (fig.8). The different sensors didn't show any response to the different vapors at temperatures below 180°C.

Above 180°C, the SnO_x gas sensor showed obvious response to ethanol, acetone and benzene with an observed higher affinity towards ethanol vapor (fig. 8). For this sensor, the optimal response to ethanol was exhibited at 180°C, thereby reaching around 70% (fig. 8a). In the same conditions, ZnO presented lower response around 28% for ethanol. On the other hand, ZnO demonstrated a higher affinity to acetone with an optimal response at 250°C reaching around 50% (fig. 8b).

Also, by comparing the response kinetics of both sensors, it's clear that the response time dropped significantly when rising the sensor temperature from 180 to 250°C (fig. 8e). Generally, ZnO demonstrated faster response kinetics towards benzene and ethanol vapors. In turn, the response time towards acetone was much faster in case of SnO_x sensor reaching about 5 s.

As reported in literature, gas sensors based on pure tin oxide or zinc oxide nanotubes or nanofibers usually show quasi similar sensitivity to ethanol and acetone due to their similar chemical nature [21-22]. The most efficient way which was proven to reduce the cross sensitivity between both vapors is by doping the metal oxide nanotube by metal nanoparticles [21] or by producing different metal oxide composites [22-23]. Furthermore, the analysis of the cross sensitivity between both vapors and benzene has not been addressed using pure tin oxide or zinc oxide nanotubes. In this work, both SnO_x and ZnO sensors demonstrated a lower sensitivity to benzene, while showing the highest response times towards this gas, in comparison to ethanol and acetone. This preliminary study suggested a

high variability of the sensing behavior of both analyzed SnO_x and ZnO sensors at different temperatures, towards the three vapors, in terms of sensing response magnitude and kinetics.
Therefore, by combining the four sensor data based on SnO_x and ZnO sensors operated at 180 and 250°C, PCA showed a good ability of the four sensor array to discriminate between the three analyzed vapors (fig.9). Moreover, since each of the three vapors is expected to take a different direction, a good separation may then be possible. These first results open the way for the simultaneous detection of the three vapors, which is not obviously possible using a single gas sensor.

4. Conclusions

In summary, pure and porous SnO_x and ZnO ultrafine tubes were successfully prepared by a simple home-made Forcespinning system with diameters in the range of 0.4-8 µm, as confirmed by FESEM, XRD, and EDS, TGA and BET analysis. The gas sensor response and response time for a variety of tested vapors were measured at different operating temperatures. The results demonstrated that the SnO_2 and ZnO sensor were sensitive to different toxic volatile organic vapors such as ethanol, acetone, and benzene with variable sensing response magnitude and kinetics. The data variability resulted in a discrimination of the three vapor patterns by combining the sensors based on both ZnO and SnO_x, as observed in PCA scatter plots.
All the above results proved the potential of the Forcespinning technology as a simple and scalable approach for preparing SnO_x and ZnO ultrafine tubes for hazardous vapor monitoring. Next work will focus on the optimization of the tube morphology and sensor response kinetics.

References

[1] S. Feng, F. Farha, Q. Li, Y. Wan, Y. Xu, T. Zhang, and H. Ning, Review on Smart Gas Sensing Technology, Sensors 19 (2019) 3760-
[2] https://www.cdc.gov/niosh/npg/npgd0004.html
[3] https://www.cdc.gov/niosh/npg/npgd0262.html
[4] https://emergency.cdc.gov/agent/benzene/basics/facts.asp
[5] G. Korotcenkov, V. Brinzari, I.A. Pronin, M.H. Ham and B.K Cho, Metal oxides for application in conductometric gas sensors : how to choose?, Solid State Phenom. 266 (2017) 187-195.
[6] Y. Xia, P. Yang, Y. Sun, Y. Wu, B. Mayers, B. Gates, Y. Yin, F. Kim, H. Yan, One-Dimensional Nanostructures : Synthesis, Characterization , and Applications, Adv. mater. 15 (5) (2003) 353–389.
[7] G. Korotcenkov and B. K. Cho, Metal oxide composites in conductometric gas sensors: Achievements and challenges, Sens. Actuators B Chem. 244 (2017)182–210.
[8] T-J. Hsueh, S-J. Chan, C-L. Hsu, Y-R. Lin and I-C. Chen, ZnO nanotube ethanol gas sensors, J. Electrochem. Soc. 155 (9) (2008) K152-K155
[9] Y. Zhang, M. Liu, W. Ren, Z-G. Ye, Well-ordered ZnO nanotube arrays and networks grown by atomic layer deposition, Appl. Surf. Sci. 340 (2015), 120-125.
[10] M. Bechelany, A. Amin, A. Brioude, D. Cornu, P. Miele, ZnO nanotubes by template-assisted sol–gel route, J. Nanopart. Res. 14 (2012) 980-.
[11] Y. Sun, D-J. Riley, M.N.R. Ashfold, Mechanism of ZnO Growth y hydrothermal methods on ZnO Film-Coated Si substrates, J. Phys. Chem. 110 (31) (2006) 15186-15192.
[12] L. Shi and H. Lin, Preparation of Band Gap Tunable SnO2 Nanotubes and Their Ethanol Sensing Properties, Langmuir 27 (7) (2011) 3977-3981.
[13] Y. Tang, L. Luo, Z. Chen, Y. Jiang, B. Li, Z. Jia, L. Xu, Electrodeposition of ZnO nanotube arrays on TCO glass substrates, Electrochem. Commun. 9 (2007) 289–292.
[14] X. Yu, F. Song, B. Zhai, C. Zheng, Y. Wang, Electrospun ZnO Nanotubes and its Gas Sensing Applications, Physica Physica E. 52 (2013) 92–96.
[15] W-S. Chen, D-A. Huang, H.C. Chen, Z-Y. Shie, C-H. Hsieh, J-D. Liao, C. Kuo, Fabrication of Polycristalline ZnO nanotubes from the electrospinning of Zn2+/poly(acrylic acid), Cryt. Growth Des. 9 (9) (2009) 4070-4077.
[16] P.M. Bulemo, H-J. Cho, N-H. Kim, Mesoporous SnO2 Nanotubes via Electrospinning–Etching Route: Highly Sensitive and Selective Detection of H2S Molecule, ACS Appl. Mater. Interfaces 9 (31) (2017) 26304-26313.
[17] L. Ren, R. Ozisik, and S. P. Kotha, Rapid and efficient fabrication of multilevel structured silica micro-/nanofibers by centrifugal jet spinning, J. Colloid Interface Sci. 425 (2014) 136–142.
[18] S. Mahalingam and M. Edirisinghe, Forming of polymer nanofibers by a pressurised gyration process, Macromol. Rapid Commun. 34 (14) (2013) 1134–1139.
[19] S. Padron, R. Patlan, J. Gutierrez, N. Santos, T. Eubanks, Production and Characterization of Hybrid BEH-PPV / PEO Conjugated Polymer Nanofibers by Forcespinning TM, J. Appl. Polym. Sci. 125 (5) (2011) 1–7.
[20] I.T. Jolliffe and J. Cadima, Principal component analysis: a review and recent developments, Philos. Trans. A Math.

Phys. Eng. Sci. 374 (2065) (2016) 20150202-.
[21] H. Lei and L. Yi, Improved acetone sensing properties of flat sensors based on Co-SnO2 composite nanofibers, Environ. Sci. Technol. 56 (24) (2011) 2644-2648.
[22] J. Wang, J. Yang, N. Han, X. Zhou, S. Gong, J. Yang, P. Hu, Y. Chen, Highly sensitive and selective ethanol and acetone gas sensors based on modified ZnO nanomaterials, Mater. Design 121 (2017) 69-77.
[23] T. Alali, JY. Liu, Q. Liu, R. Li, HQ. Zhang, K. Aljebawi, P. Liu, J. Wang, Enhanced acetone gas sensing response of ZnO/ZnCo2O4 nanotubes synthesized by single capillary electrospinning technology, Sens. Actuator. B-Chem. 252 (2017) 511-522.

Figure captions

Fig.1: Home-made Forcespinning system used for MOs fiber formation

Fig. 2 (a) Experimental gas sensor characterization circuit (b) gas sensing platform

Fig.3: FESEM images of (a) $SnCl_2$/PVP composite fibers (b) annealed SnO_x tubes (c) Zn $[COOCH3]_2$/PVP composite fibers (d) annealed ZnO tubes (e) Tube diameter distribution histogram for SnO_x tubes (f) ZnO tubes

Fig.4: TGA/DTA curves of (a) as-spun SnCl/PVP and (b) Zn $[COOCH_3]_2$/ PVP samples

Fig 5. EDS analysis for (a) SnO_x and (b) ZnO

Fig.6: XRD patterns of (a) SnO_x (b) ZnO

Fig. 7: Nitrogen adsorption isotherms for (a) SnO_x (b) ZnO tubes

Fig.8: (a-c) Example of Sensor dynamic response versus time of SnO2 and ZnO tubes towards VOCs (d) Histogram of response magnitude (e) Histogram of response time at different temperatures

Fig.9: Individuals PCA scatter plot showing the discrimination of the three vapor patterns

Figure 1

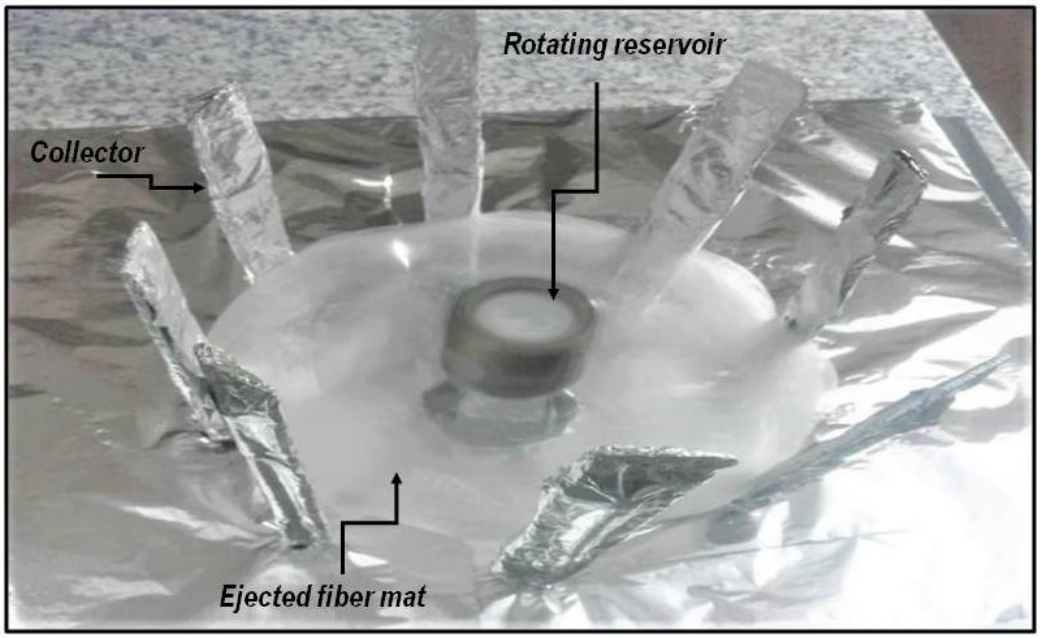

Figure 2

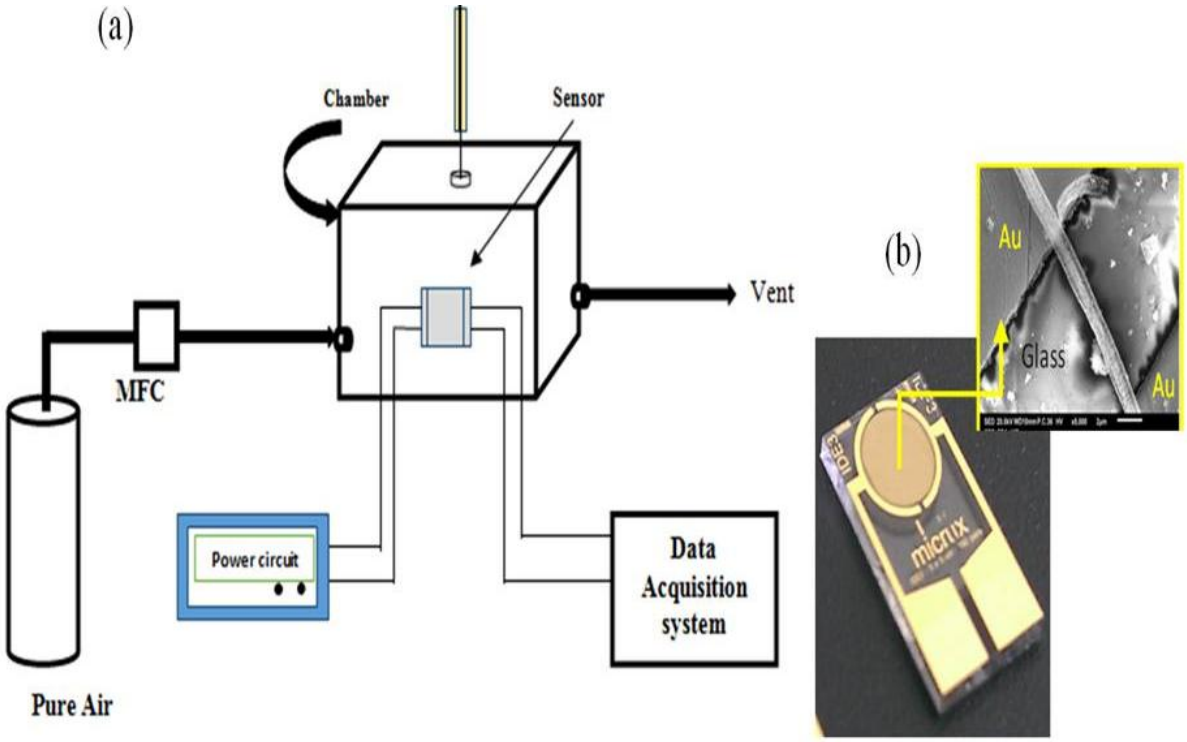
(a)
Chamber
Sensor
Vent
MFC
Power circuit
Data Acquisition system
Pure Air
(b)
Au
Glass
Au

Figure 3

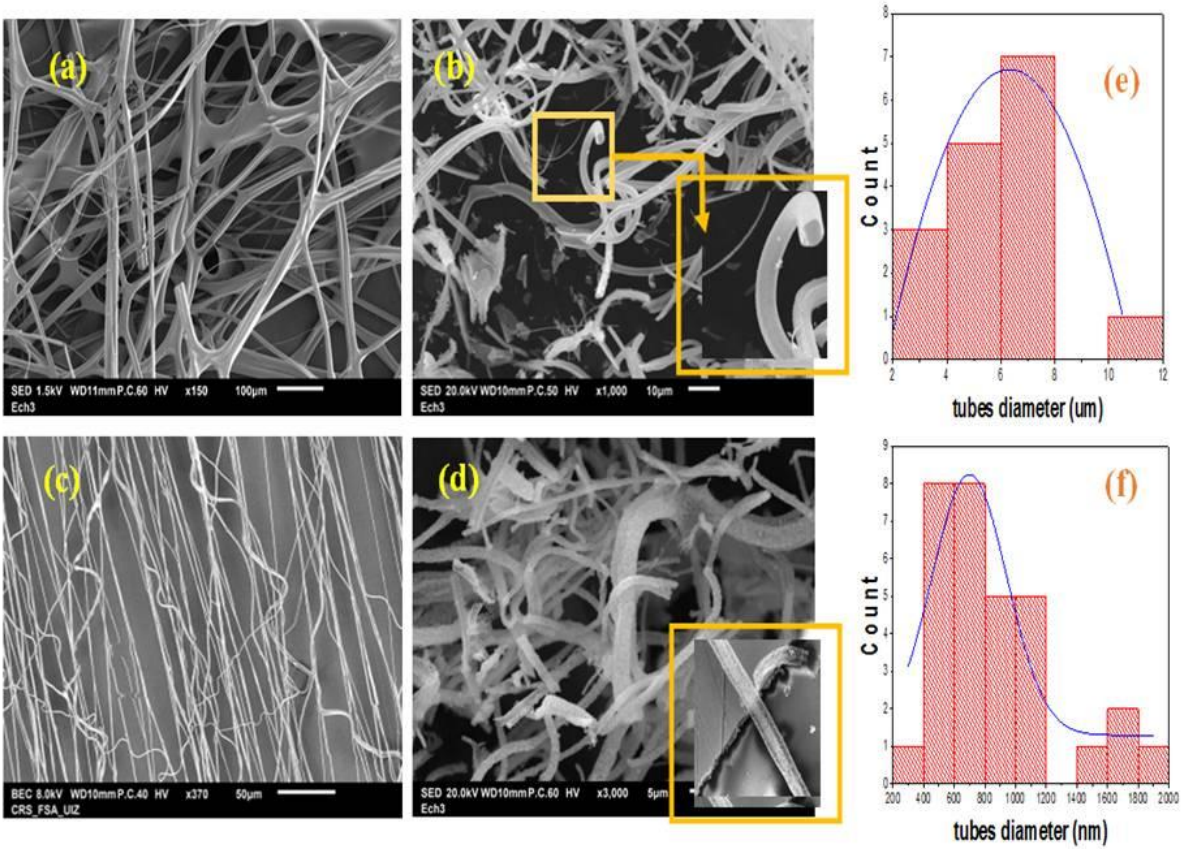
(a)
SED 1.5kV WD11mmP.C.60 HV x150 100µm
Ech3
(b)
SED 20.0kV WD10mmP.C.50 HV x1,000 10µm
Ech3
(e)
Count
tubes diameter (um)
(c)
BEC 8.0kV WD10mmP.C.40 HV x370 50µm
CRS_FSA_UIZ
(d)
SED 20.0kV WD10mmP.C.60 HV x3,000 5µm
Ech3
(f)
Count
tubes diameter (nm)

Figure 4

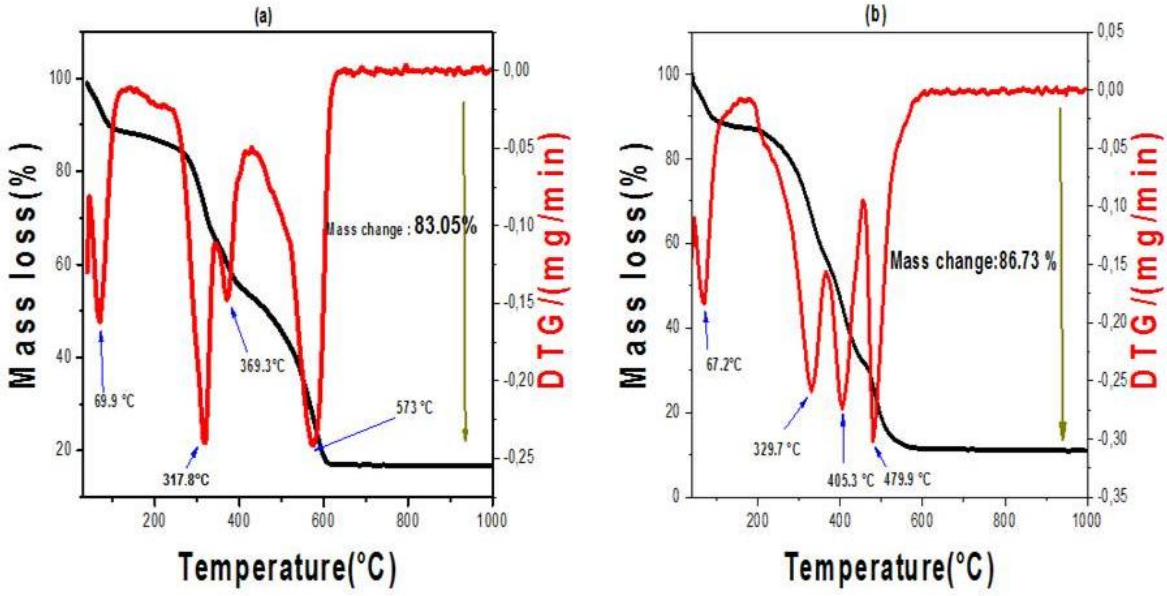
(a)
Mass loss(%)
DTG/(mg/min)
Temperature(°C)
Mass change : 83.05%
69.9 °C
317.8°C
369.3°C
573 °C
(b)
Mass loss(%)
DTG/(mg/min)
Temperature(°C)
Mass change:86.73 %
67.2°C
329.7 °C
405.3 °C
479.9 °C

Figure 5

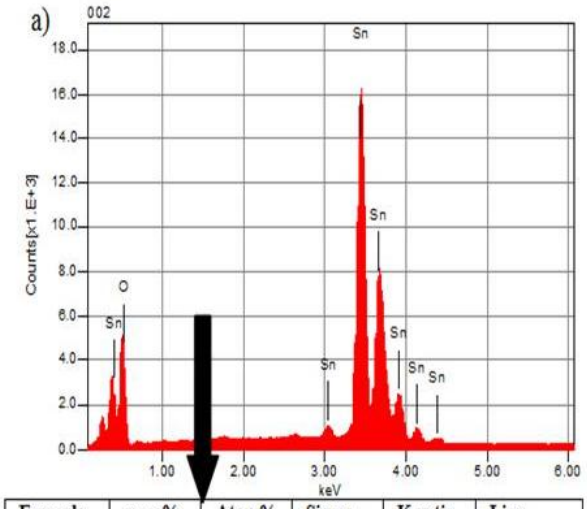

Formula	mass%	Atom%	Sigma	K ratio	Line
O	5.01	28.13	0.01	81456	0.0638536
Sn	94.99	71.87	0.14	941299	0.6770406
Total	100	100			

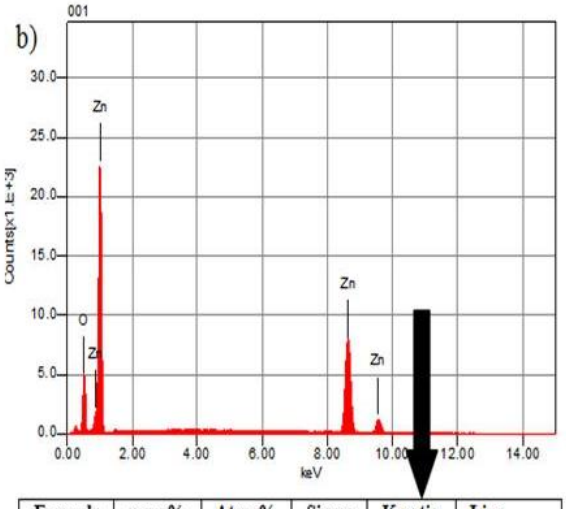

Formula	mass%	Atom%	Sigma	K ratio	Line
O	10.31	31.97	0.02	87078	0.0682608
Zn	89.69	68.03	0.15	417019	0.8157049
Total	100	100			

Figure 6

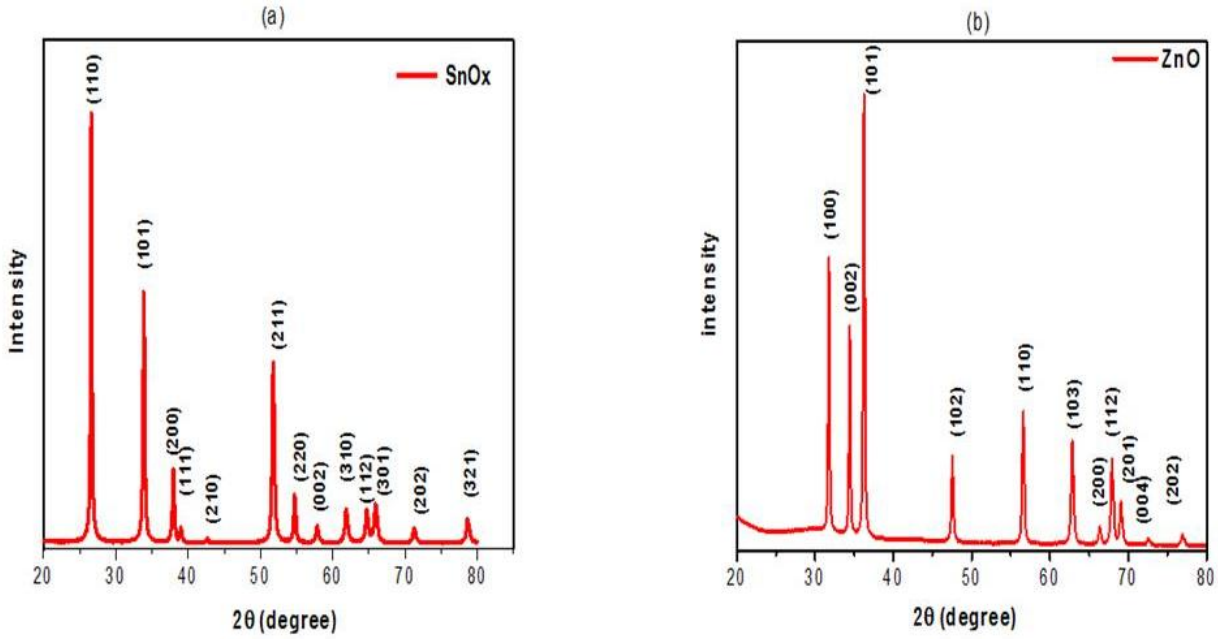
(a)
SnOx
(110)
(101)
(200)
(111)
(210)
(211)
(220)
(002)
(310)
(112)
(301)
(202)
(321)
Intensity
20
30
40
50
60
70
80
2θ (degree)
(b)
ZnO
(100)
(002)
(101)
(102)
(110)
(103)
(200)
(112)
(201)
(004)
(202)
intensity
20
30
40
50
60
70
80
2θ (degree)

Figure 7

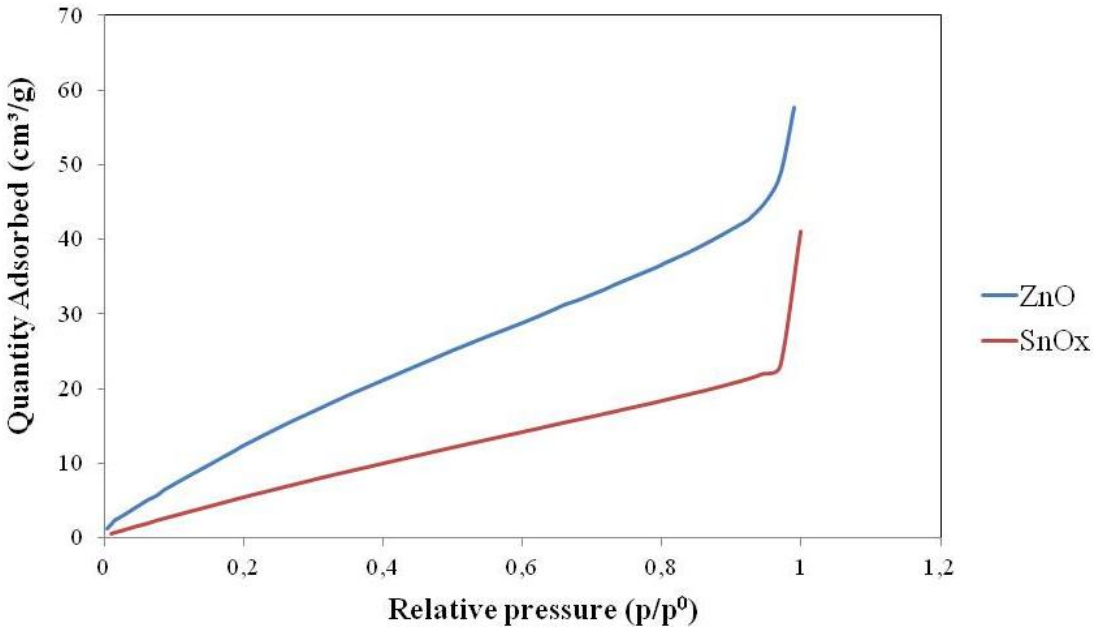
70
60
50
40
30
20
10
0
Quantity Adsorbed (cm³/g)
0
0,2
0,4
0,6
0,8
1
1,2
Relative pressure (p/p⁰)
ZnO
SnOx

Figure 8

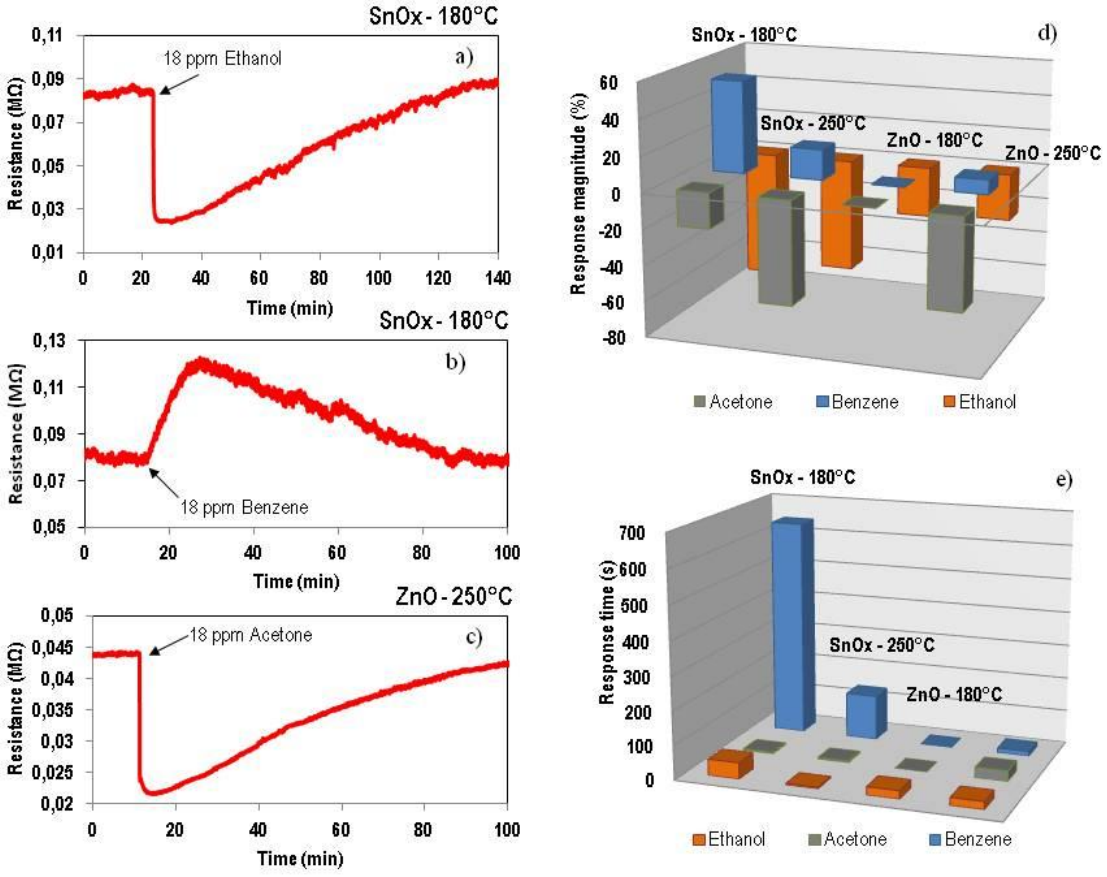
SnOx - 180°C
18 ppm Ethanol
a)
Resistance (MΩ)
Time (min)
SnOx - 180°C
b)
18 ppm Benzene
Resistance (MΩ)
Time (min)
ZnO - 250°C
18 ppm Acetone
c)
Resistance (MΩ)
Time (min)
SnOx - 180°C
d)
SnOx - 250°C
ZnO - 180°C
ZnO - 250°C
Response magnitude (%)
Acetone
Benzene
Ethanol
SnOx - 180°C
e)
SnOx - 250°C
ZnO - 180°C
Response time (s)
Ethanol
Acetone
Benzene

Figure 9

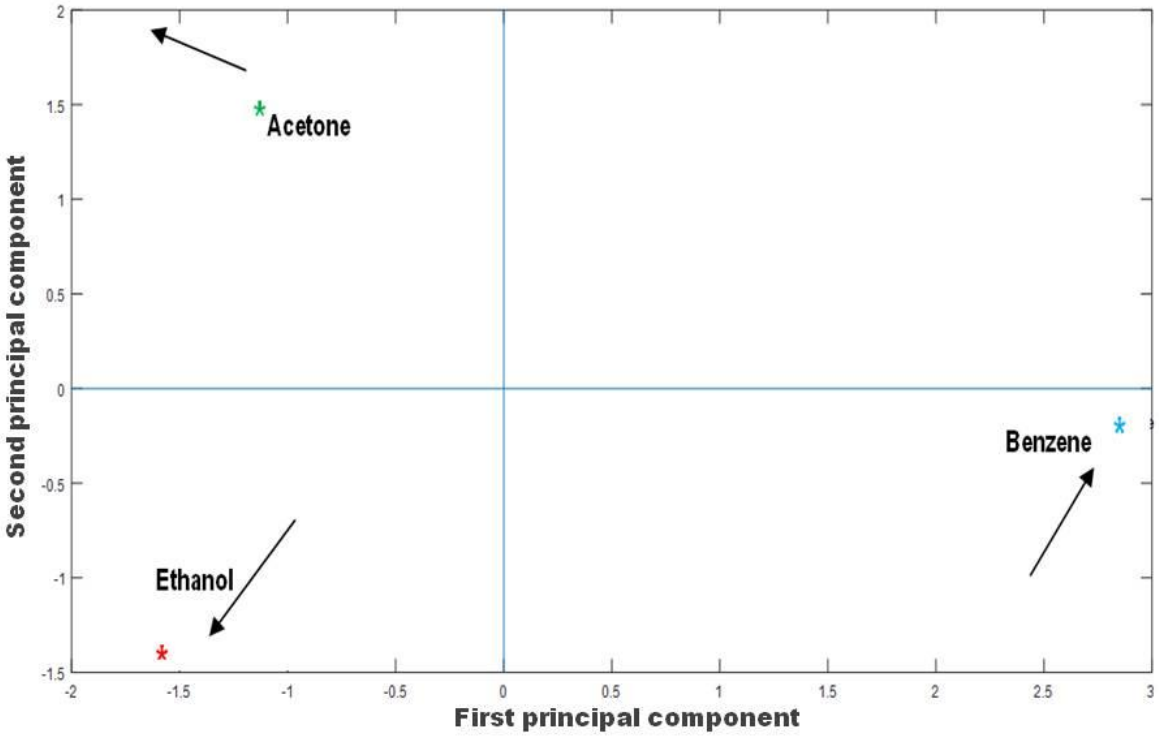
Acetone
Benzene
Ethanol
Second principal component
First principal component
2
1.5
1
0.5
0
-0.5
-1
-1.5
-2
-1.5
-1
-0.5
0
0.5
1
1.5
2
2.5
3